Applied Catalysis B: Environmental 119–120 (2012) 279–286

Contents lists available at SciVerse ScienceDirect

Applied Catalysis B: Environmental

journal homepage: www.elsevier.com/locate/apcatb

NO_x storage and reduction over flame-made $M/MgAl_2O_4$ (M = Pt, Pd, and Rh): A comparative study

Sounak Roy[a], Niels van Vegten[a], Nobutaka Maeda[a], Alfons Baiker[a,b,*]

[a] Institute for Chemical and Bioengineering, Department of Chemistry and Applied Bioscience, ETH, Zurich, Hönggerberg, HCI, CH-8093 Zurich, Switzerland
[b] Chemistry Department, Faculty of Science, King Abdulaziz University, P.O. Box 80203, Jeddah 21589, Saudi Arabia

ARTICLE INFO

Article history:
Received 22 December 2011
Received in revised form 2 March 2012
Accepted 6 March 2012
Available online 14 March 2012

Keywords:
NO_x storage and reduction
Platinum
Palladium
Rhodium
$MgAl_2O_4$
Spinel
Dynamic cycling behavior
Time-resolved IR spectroscopy

ABSTRACT

Various NO_x storage–reduction (NSR) catalysts with 1 wt% noble metal loading (Pt, Pd, or Rh) dispersed on $MgAl_2O_4$ have been synthesized by single step flame spray pyrolysis. The as-prepared powders consisting of nonporous nanoparticles were characterized by X-ray diffraction, scanning transmission electron microscopy, nitrogen adsorption–desorption, CO chemisorption and thermogravimetric methods. Different reduction agents were applied in the fuel rich cycles: H_2, CO or C_3H_6. Processes occurring during fuel rich and lean cycles were analyzed in detail by means of time-resolved diffuse reflectance infrared Fourier transform spectroscopy (DRIFTS), and thermogravimetry combined with mass spectroscopy. With H_2 as reductant, $Pt/MgAl_2O_4$ showed the best performance at short regeneration time (<50 s), followed by $Rh/MgAl_2O_4$ and $Pd/MgAl_2O_4$. However, if CO or C_3H_6 were used as reductant, $Rh/MgAl_2O_4$ outperformed both other catalysts, especially at longer regeneration times (>50 s). NO_x storage on these catalysts was mainly restricted to surface species, although bulk nitrate species were identified by DRIFTS as well. The latter were not completely reduced under the experimental conditions used.

1. Introduction

One of the most promising and efficient techniques for NO_x removal from lean burn engines is NO_x storage and reduction (NSR). Since Toyota introduced the ground laying NSR catalyst $Pt–Ba/Al_2O_3$, many investigations have focused on the understanding of the functioning of this catalyst type and further improvement of its efficiency [1–4]. Some deficiencies of these catalysts that still need further improvement are: (i) under realistic conditions, particularly at short regeneration times, storage performance deteriorates with time (from cycle to cycle) due to incomplete reduction of bulk barium nitrates which are partially inaccessible during the subsequent lean phase [5–11], (ii) deterioration of the storage performance is observed with Ba containing catalyst due to mixed oxide formation at high temperatures [12,13], (iii) sulfur poisoning [14,15], and (iv) poisoning of the noble metal sites in presence of carbonaceous reductants (like CO, and hydrocarbons) and CO_2 [16–19]. In an earlier investigation, we showed that a flame-made 1 wt% $Pt/MgAl_2O_4$ catalyst had superior dynamic performance in NO_x storage–reduction at short regeneration times (<30 s) compared to a standard 1 wt% Pt – 20 wt% Ba/Al_2O_3 reference catalyst [20]. However, the better NSR performance at short regeneration times of $Pt/MgAl_2O_4$ was limited to the use of hydrogen as reductant, whereas with other reductants, CO or hydrocarbons, the NSR performance was similar for both catalysts.

Generally, the NSR mechanism can be considered to involve three main steps which occur during cycling between lean and rich periods: these are NO oxidation to NO_2 and NO_x storage by the alkali- or earth alkaline-component during the fuel lean period, and reduction of released NO_x to N_2 by the reductants during the fuel rich period [3,4].

Platinum, palladium, and rhodium as well as bimetallic systems therefore have proven to be most suitable noble metal components for NSR catalysts [3,4]. Abdulhamid et al. [21] investigated the storage and reduction of NO_x over $BaCO_3/Al_2O_3$ supported Pt, Pd, and Rh catalysts using CO, H_2, C_3H_6, or C_3H_8 as the reducing agent. They found that using CO as the reductant results in a lower NO_x reduction capacity for $Pt/BaCO_3/Al_2O_3$ compared with Pd- and Rh-based samples, whereas H_2 shows a significant ability to reduce the stored NO_x on all these catalysts. The reduction with CO and C_3H_6 proceeded via the formation of isocyanate species over both barium and alumina sites.

The aim of the present study was the elucidation of the NSR performance of different flame-made noble metals supported on

* Corresponding author at: Institute for Chemical and Bioengineering, Department of Chemistry and Applied Bioscience, ETH, Zurich, Hönggerberg, HCI, CH-8093 Zurich, Switzerland. Tel.: +41 44 632 3153; fax: +41 44 632 1163.
E-mail address: baiker@chem.ethz.ch (A. Baiker).

0926-3373/$ – see front matter © 2012 Elsevier B.V. All rights reserved.
doi:10.1016/j.apcatb.2012.03.008

$MgAl_2O_4$ spinel. Three different $M/MgAl_2O_4$ (M = Pt, Pd, or Rh) catalysts were synthesized, structurally characterized and tested with regard to their overall efficiency in lean-rich cycling experiments. Different model reductants, H_2, CO, and propene, were employed to mimic the fuel rich condition cycle in NSR. Finally, we gained some insight into the NO oxidation, NO_x storage, and the reduction behavior of the stored NO_x by time-resolved DRIFT spectroscopy.

2. Experimental

The catalysts were synthesized by flame spray pyrolysis (FSP) [22,23]. Precursor solutions were made from aluminum acetylacetonate, Mg(II)tert-butoxide, Pt(II)acetylacetonate, Rh(III) acetylacetonate and Pd(III) acetylacetonate, dissolved in a 1:1 vol.% mixture of methanol and acetic acid and were fed at 5 mL min^{-1} through the nozzle using a syringe pump. The noble metal loading of all catalysts was 1 wt%. The particles formed were collected on a glass fiber filter with the aid of a vacuum pump.

The structural properties of the synthesized powders were characterized by X-ray diffraction, scanning transmission electron microscopy (STEM), CO chemisorption and nitrogen adsorption measurements using the BET method. X-ray diffraction was carried out on a Siemens D5000 diffractometer, using $CuK_{\alpha 1}$ (λ = 1.54056 Å) in step mode from 15° to 65° (2θ) with 0.01° step size and 0.3 s $step^{-1}$. For STEM the materials were dispersed in ethanol and deposited onto a perforated carbon foil supported on a copper grid. The investigations were performed on a Tecnai F30 microscope (FEI (Eindhoven); field emission cathode, operated at 300 kV).

CO chemisorption was performed using a Micromeritics ASAP 2010C instrument. The sample was exposed to a flow of hydrogen at 350 °C for 1 h and then evacuated at the same temperature. Two chemisorption isotherms were then measured at room temperature. The first isotherm corresponds to all carbon monoxide adsorbed on the catalyst. After evacuation at the same temperature for 1 h, the second isotherm was measured, corresponding to the weakly adsorbed CO. From the difference between the two isotherms, the fraction of strongly adsorbed (chemisorbed) CO was determined and metal dispersions were derived from these values using a stoichiometric factor of 1 for Pt and Pd. Due to the uncertainty in the stoichiometric factor and possible surface reconstruction the Rh dispersion could not be reliably determined from CO chemisorption. The mean particle size was therefore estimated from STEM images.

Nitrogen physisorption isotherms (adsorption–desorption branches) were measured on a Micromeritics ASAP 2000 instrument at 77 K. Samples were outgassed under vacuum at 150 °C before measurement and the specific surface area (SSA) was determined using the BET method.

The NSR experiments were carried out isothermally at 350 °C with 100 mg of the 100–200 μm sieve fraction of the catalysts in a vertically placed plug-flow quartz reactor of 4 mm inner diameter. Temperature was calibrated by positioning a thermocouple in the center of the reactor. The gases were introduced via mass flow controllers at a total flow rate of 120 cm^3 min^{-1} (corresponding to a GHSV of ca. 36,000 h^{-1}), and the effluent gases were analyzed using a mass spectrometer (Thermostar™, Pfeiffer Vacuum). The reactor was connected to a valve, which allowed rapid switching between oxidizing (fuel lean) and reducing (fuel rich) atmospheres. The rich period consisted of 5 vol.% H_2/He or CO/He or C_3H_6/He (varied from 10 s to 120 s), while the lean period consisted of 1000 ppm of NO in 6.6 vol.% O_2/He (for 360 s). The specific reaction conditions used are specified in their respective places. NO_x storage, or NO_x removal, is given as percentage of the NO_x fed to the reactor, and was calculated by subtracting the integrated intensity of m/z = 30 (NO) obtained during cycling from that of the by-pass (no storage).

Time-resolved in situ diffuse reflectance infrared Fourier transform (DRIFT) spectroscopy was employed to monitor the catalytic solid–gas interface during NSR cycles by using a home-build plug-flow cell [20,24]. DRIFT spectra were measured on a Bruker Equinox 55 spectrometer equipped with a liquid nitrogen-cooled MCT detector at 4 cm^{-1} resolution. The surface processes during NO oxidation and storage were investigated by flowing 1000 ppm of NO + 6.6 vol.% O_2 in He balance over the catalysts at 350 °C. The NO_x reduction process was then monitored during exposure of the catalyst to flowing 5 vol.% H_2/He, 5 vol.% CO/He or 5 vol.% C_3H_6/He.

Thermogravimetric experiments were performed on a Netzsch 449C Jupiter system. Typically, between 35 and 100 mg of sample was used. Temperature programmed desorption (TPD) or oxidation (TPO) were performed by flowing 50 cm^3 min^{-1} He or 20 vol.% O_2/He, respectively, over the sample. A heating rate of 10 K min^{-1} was used, unless specified otherwise. The exhaust gas was analyzed by mass spectrometry. The NO_x storage and reduction characteristics were studied gravimetrically as well. To evaluate the maximal NO_x storage capacity, 6 cm^3 (STP) NO and O_2 injections were admitted to the He purge gas at 250 °C. Injection resulted in a sudden mass increase due to adsorption of NO_x, followed by a decrease due to partial desorption. Injections were made until further injection did not result in a permanent mass increase. The thermal stability of the stored NO_x was analyzed by TPD up to 650 °C.

3. Results and discussion

3.1. Structural properties and morphology of flame-made catalysts

Inspection of the nitrogen adsorption–desorption isotherms of the flame-derived powders confirmed that they were virtually non-porous, showing only some small hysteresis at p/p_o close to 1 due to the interparticle void volume of the powders. The specific surface areas (SSAs) of the as-prepared materials are listed in Table 1. $MgAl_2O_4$ supported Pt showed a higher SSA with 226 m^2 g^{-1} compared to corresponding Rh and Pd catalysts, for which 193 m^2 g^{-1} were measured. Since all these materials were synthesized under identical conditions (precursor concentrations resulting in 1 wt% metal loading, flame-settings etc.), the difference in SSAs is likely the result of the different interactions between the noble metals and Mg and Al in the flame during particle formation. Similar effect of the noble metal has been reported before for Pt [25] and Pd [26] based catalysts.

X-ray diffraction of the as-prepared materials showed the $MgAl_2O_4$ support to be present in the spinel crystalline phase in all three synthesized powders (JCPDS 05-0672, see Fig. 1). The mean crystallite sizes derived from the full width at half maximum (FWHM) of the (3 1 1) reflection at around 37° (2θ) are listed in Table 1. $Pd/MgAl_2O_4$ and $Rh/MgAl_2O_4$ had rather comparable $MgAl_2O_4$ crystallite sizes (ca. 9 nm), whereas the same constituent in $Pt/MgAl_2O_4$ showed a slightly lower crystallite size (8 nm). These

Table 1
Structural properties of 1 wt% $M/MgAl_2O_4$ catalysts (M = Pt, Pd or Rh).

Catalyst	SSA (m^2 g^{-1})	d_{XRD}[a] (nm)	Mass loss[b] (wt%)	CO/M[c]
$Pt/MgAl_2O_4$	226	8.0	8.12	0.13
$Pd/MgAl_2O_4$	193	9.8	7.49	0.28
$Rh/MgAl_2O_4$	193	9.4	7.49	0.75[d]

[a] Crystallite size estimated from XRD-line broadening of (3 1 1) reflection.
[b] Mass loss after heating to 550 °C at 15 K min^{-1} in 20% O_2/He.
[c] CO to total noble metal atom ratio. Assuming a stoichiometric factor of 1 for Pt and Pd these values represent the dispersions of these metals.
[d] Due to some uncertainty in the stoichiometric factor, the Rh dispersion was not determined from CO chemisorption. It was estimated from the mean particle size determined from STEM images to be around 0.5.

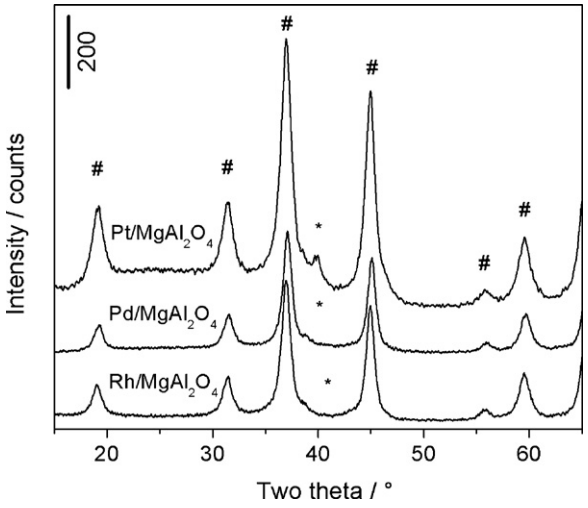

Fig. 1. XRD patterns of flame-made 1 wt% M/$MgAl_2O_4$ (M = Pt, Pd, or Rh) catalysts. #$MgAl_2O_4$ and and * marks expected two theta positions of (111) reflections of noble metals.

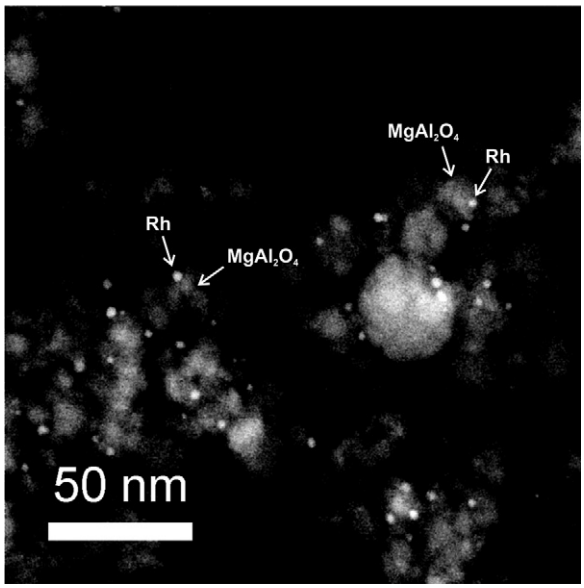

Fig. 2. Typical STEM images of Rh/$MgAl_2O_4$. STEM images of Pt/$MgAl_2O_4$ are given in Ref. [20].

findings are in line with the observed differences in SSA. X-ray diffraction of both Pd/$MgAl_2O_4$ and Rh/$MgAl_2O_4$ did not reveal any noble metal-related reflections due to the low metal loading (1 wt%) and the small particle size. Pt/$MgAl_2O_4$ on the other hand, showed a small feature around 40° (2θ), which points to the presence of larger Pt crystallites, in line with the lower metal dispersion of this catalyst.

To gain some information about the dispersion of the noble metal constituent, CO chemisorption measurements were performed. The CO/M_{tot} ratios measured are listed in Table 1. The lowest CO/M_{tot} ratio was obtained for Pt/$MgAl_2O_4$ (0.13), followed by Pd/$MgAl_2O_4$ (0.28) and Rh/$MgAl_2O_4$ (0.75). Note that the average CO to surface noble metal atom ratio ($CO/M_{surface}$) depends not only on the metal, but also on the size and shape of the metal particles under investigation [27]. For a rough comparison of the metal dispersions we assumed a stoichiometric factor of 1 for Pt and Pd. Determination of the Rh dispersion from CO chemisorption suffers from uncertainty of the stoichiometric factor and possible surface reconstruction, therefore the mean Rh particle size was estimated from STEM images.

Previous STEM investigations [20] revealed that Pt and $MgAl_2O_4$ were predominantly present as particles of less than 5 nm and 12 nm size, respectively. However, also some larger Pt (~10 nm) and $MgAl_2O_4$ (>50 nm) particles were observed. In contrast, the sizes of noble metal and support particles were more uniform in Pd/$MgAl_2O_4$ and Rh/$MgAl_2O_4$. Rh particles were around 2 nm (Fig. 2), although the low contrast between the particles and the support rendered accurate analysis difficult. In Pd/$MgAl_2O_4$, the Pd particles were around 4 nm in size.

Analysis of the SSA and mean crystal size of the $MgAl_2O_4$ constituent (Table 1, Fig. 1) indicates rather similar structural properties. The higher SSA of Pt/$MgAl_2O_4$ is in line with its slightly smaller crystal size compared to the Pd/$MgAl_2O_4$ and Rh/$MgAl_2O_4$. Differences were also observed in the noble metal dispersions (Table 1). It has earlier been observed that the surface properties are of paramount importance for NSR on $MgAl_2O_4$-based catalysts [20], and therefore the samples were further characterized by temperature programmed desorption (TPD) and oxidation (TPO).

Initial TPD experiments by TG–MS (see Section 2), showed significant evolution of H_2 (m/z = 2) and an erratic CO_2 signal (m/z = 44) between ca. 290 and 700 °C. In the same temperature range, the O_2 signal (m/z = 32) dropped measurably. These two events indicate the presence of a hydrocarbon-based residue on the surface of the catalysts. The likely sources of this residue are un-burnt solvent or organic precursor residues from the flame pyrolysis which reacted with the trace oxygen present in the He feed stream and were partially oxidized. To circumvent the erratic signal resulting from this partial oxidation reaction, TPO experiments were performed instead. The weight-loss up to 550 °C is listed in Table 1. Pt/$MgAl_2O_4$ showed a slightly higher weight-loss compared to those of Pd/$MgAl_2O_4$ and Rh/$MgAl_2O_4$, likely it accommodated more adsorbed species (water, carbonates, nitrates and carbonaceous residue) by virtue of its higher SSA. Both Rh/$MgAl_2O_4$ and Pd/$MgAl_2O_4$ showed comparable weight-loss.

3.2. NSR performance

NO_x storage and reduction experiments over the three different noble metal catalysts were performed with H_2 and with carbonaceous reductants (CO, propene). The fuel lean period was kept constant at 6 min, whereas the fuel rich period was varied from 10 s, 20 s, 30 s, 60 s to 120 s. Fig. 3 shows the NSR

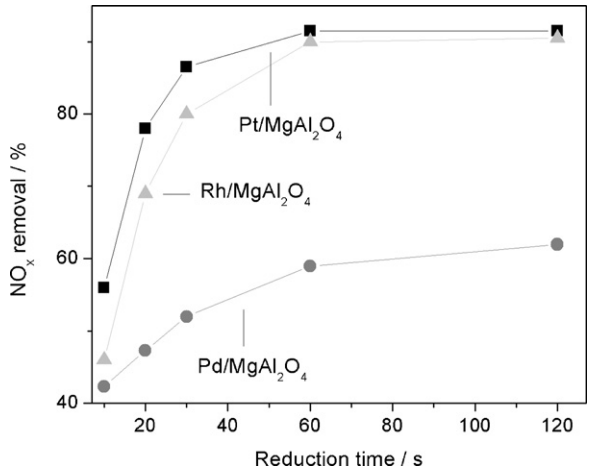

Fig. 3. NO_x storage–reduction during lean-rich cycling at 350 °C over 1 wt% M/$MgAl_2O_4$ (M = Pt, Pd, or Rh) with different duration of rich period using H_2 as reductant. The NSR cycles were carried out with 360 s lean and 10, 20, 30, 60 and 120 s rich periods. The NO_x removal plotted is that obtained after 10 steady cycles.

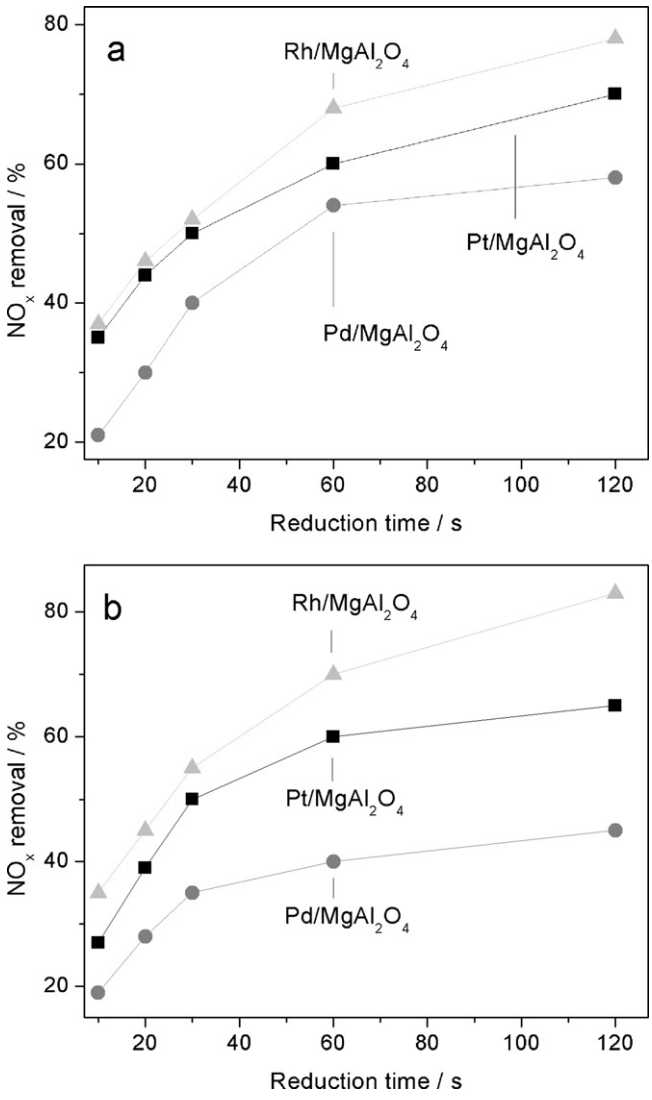

Fig. 4. NO_x storage–reduction during lean-rich cycling at 350 °C over 1 wt% $M/MgAl_2O_4$ (M = Pt, Pd, or Rh) with different duration of rich period using CO (a) and C_3H_6 (b) as reductant. The NSR cycles were carried out with 360 s lean and 10, 20, 30, 60 and 120 s rich periods. The NO_x removal plotted is that obtained after 10 steady cycles.

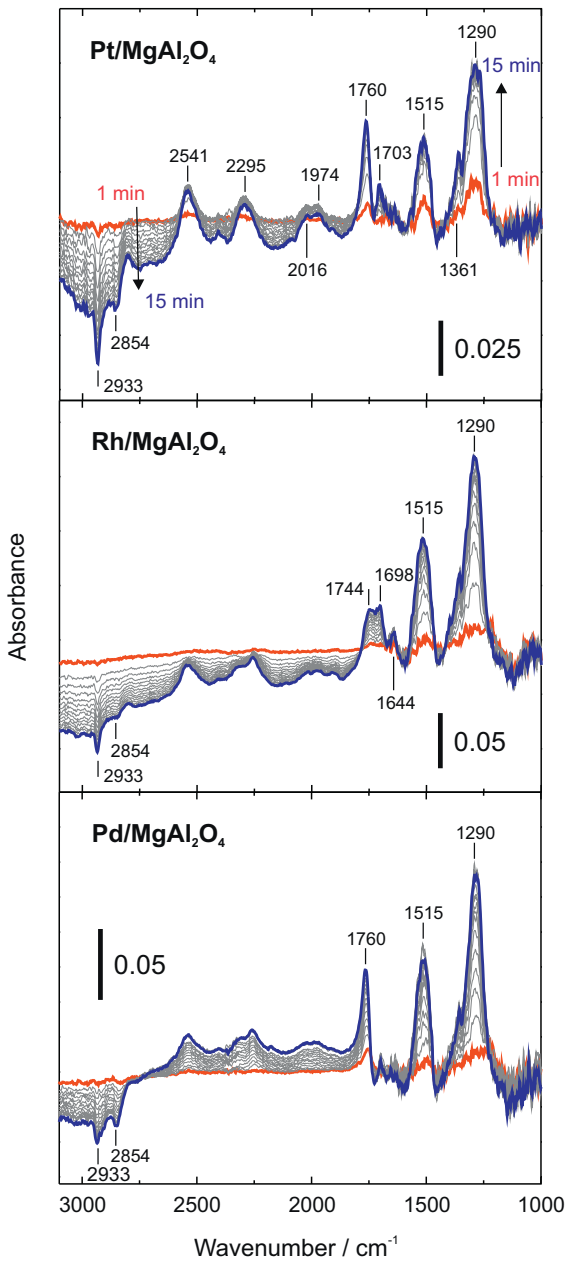

Fig. 5. Time-resolved DRIFT spectra (1–15 min) during lean period (1000 ppm NO + 6.6 vol.% O_2 in He balance) over 1 wt% $M/MgAl_2O_4$ (M = Pt, Pd, or Rh) at 350 °C (Color on Web).

performance of $M/MgAl_2O_4$ (M = Pt, Pd, and Rh) in terms of NO_x removal ability, using H_2 as reductant. $Pt/MgAl_2O_4$ showed the best performance at short reduction (regeneration) time (<50 s), followed by $Rh/MgAl_2O_4$ and $Pd/MgAl_2O_4$. However, at longer regeneration time, Pt and $Rh/MgAl_2O_4$ showed similar NO_x removal. $Pd/MgAl_2O_4$ showed by far the lowest efficiency among these three catalysts.

Figure 4 shows NSR performance with CO (Fig. 4a) and C_3H_6 (Fig. 4b) in terms of NO_x removal. Interestingly, $Rh/MgAl_2O_4$ exhibited highest NO_x removal among the three catalysts. The order of efficiency is: $Rh/MgAl_2O_4 > Pt/MgAl_2O_4 > Pd/MgAl_2O_4$. Note that at short reduction time (<30 s), i.e. where the contact time of CO with the catalysts is short, the differences in the NSR performance was small between $Pt/MgAl_2O_4$ and $Rh/MgAl_2O_4$, while at longer reduction time the activity differences were more prominent (Fig. 4a). With propene as reductant the differences in the NSR performance were prominent even at short regeneration times (<30 s). The different NSR behavior of the noble metal catalysts with H_2 (Fig. 3) and carbonaceous (CO, propene) reducing agents (Fig. 4a and b) is attributed to the fact that the metals show different intrinsic activities for NO_x reduction depending on the reducing agent applied. Furthermore, with the carbonaceous reductants the NO_x reduction mechanism is complicated by the involvement of several carbon containing species, which are absent when H_2 is used as reductant.

The results shown in Fig. 3 inspired us to investigate the separate steps of NO oxidation, and NO_x storage and reduction over these three catalysts in more detail.

3.3. Nitrate formation

To gain insight into the processes occurring at the catalytic solid–gas interface, time-resolved in situ DRIFT spectra were measured during the NO_x storage period (1000 ppm NO + 6.6 vol.% O_2 in He balance) at 350 °C. As seen in Fig. 5 (top), several fundamental, overtone and combination bands assignable to $Mg(NO_3)_2$ were

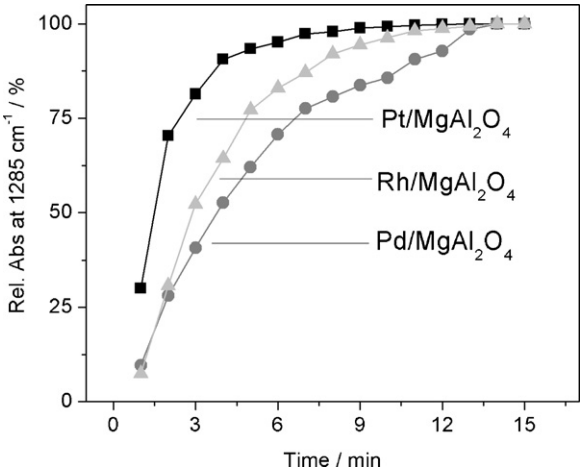

Fig. 6. Nitrate formation with time during lean period measured as relative intensity of 1290 cm^{-1} band with time over 1 wt% $M/MgAl_2O_4$ (M = Pt, Pd, or Rh) at 350 °C.

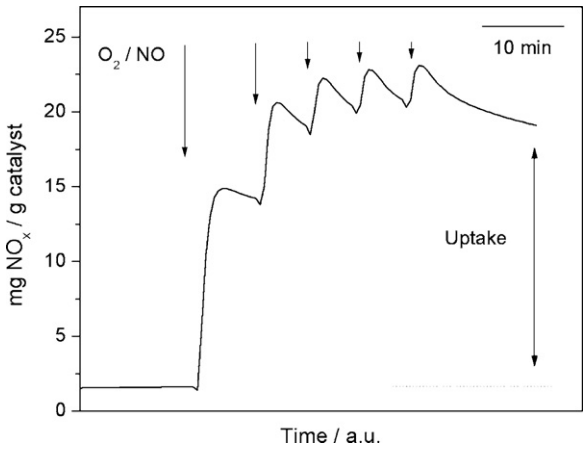

Fig. 7. Gravimetrically monitored uptake of NO_x at 250 °C over $Rh/MgAl_2O_4$.

observed on $Pt/MgAl_2O_4$; the symmetric stretching vibration (ν_3) at 1361 cm^{-1}, $\nu_1 + \nu_4$ at 1760 cm^{-1}, overtones of symmetric stretching vibration (ν_1) at around 2000 cm^{-1}, $\nu_1 + \nu_3$ at 2295 cm^{-1}, overtone of ν_3 at 2541 cm^{-1}. All these bands indicate the presence of bulk nitrate species [28]. Since XRD measurements showed no diffraction patterns of $Mg(NO_3)_2$ [20], it seemed to form small particles or multi-layers over the surface. Besides, surface nitrate species were also observed such as bridging bidentate (1703 cm^{-1}) [29–32] and chelating bidentate nitrates (1290 and 1515 cm^{-1}) [31]. The spectral feature for $Pd/MgAl_2O_4$ was almost identical to that of $Pt/MgAl_2O_4$. However, $Rh/MgAl_2O_4$ showed different IR spectra; the combination mode of $\nu_1 + \nu_4$ shifted toward lower wavenumber and split into two bands. These splitting bands are characteristic of multi-layers of the nitrates [28]. Since no intense band at 1760 cm^{-1} was detected, $Rh/MgAl_2O_4$ is considered to form a surface $Mg(NO_3)_2$ layer by the NO_x adsorption. A common feature of all catalysts is that chelating bidentate nitrate species (1290 and 1515 cm^{-1}) dominate the surface.

It is noteworthy that upon the NO_x storage, the spectral region above 2800 cm^{-1} (C—H stretching vibrations) showed negative absorbance for all the catalysts. This indicates considerable amounts of hydrocarbonaceous species present on the surface before flowing NO and O_2. The hydrocarbonaceous species originate from unburned organic residues from the FSP synthesis. As previously reported [20], the FSP-made catalysts exhibited better NSR performance than a conventional $Pt–Ba/Al_2O_3$ catalyst despite the presence of surface carbonaceous species. Therefore, their presence on the surface can be assumed to have no significant negative influence on the catalytic cycles.

From the above discussion it is clear that the most intense NO_x-related band on the three catalysts lies at 1290 cm^{-1}, which is assigned to chelating bidentate nitrate. We therefore consider this band as a measure for the rate of nitrate formation (NO_x oxidation and subsequent adsorption) on the catalysts. Fig. 6 shows the evolution of this species expressed by the relative band area centered at 1290 cm^{-1} as a function of time. Obviously nitrate formation took place most rapidly over $Pt/MgAl_2O_4$, followed by $Rh/MgAl_2O_4$ and $Pd/MgAl_2O_4$. Note that this order coincides with the known potential of these noble metals for NO_x oxidation [3,4].

3.4. NO_x storage

Quantification of the amount of adsorbed NO_x was achieved gravimetrically (see Section 2). Fig. 7 shows a typical uptake profile obtained after subjecting $Rh/MgAl_2O_4$ to several NO/O_2 injections at 250 °C. This temperature was chosen to determine the maximal amount of NO_x which could be adsorbed on the samples. Preliminary experiments revealed that at higher temperatures a slow but constant weight-loss occurred due to desorption of NO_x, but that at 250 °C this process was sufficiently slow to obtain a stable TG trace after saturation. The final uptakes are reported in Table 2. $Pt/MgAl_2O_4$ adsorbed 25 mg $NO_x/g_{catalyst}$, more than $Pd/MgAl_2O_4$ and $Rh/MgAl_2O_4$, which both adsorbed 20 mg $NO_x/g_{catalyst}$. The higher uptake of $Pt/MgAl_2O_4$ is attributed to the higher oxidation activity and the higher SSAs of this material compared to the other catalysts. However, since NSR and DRIFTS experiments throughout this work were performed at 350 °C, quantification of the adsorbed NO_x at this temperature was required as well. Since no stable TG signal was obtained (see argumentation above), the amount of NO_x adsorbed after 30 min, just prior to reduction (vide infra), was taken as a measure of the amount of strongly adsorbed NO_x. As expected, these amounts were lower than those measured at 250 °C. Interestingly, $Pd/MgAl_2O_4$ adsorbed most NO_x, around 10 mg/$g_{catalyst}$, followed closely by $Pt/MgAl_2O_4$ with 9 and $Rh/MgAl_2O_4$ with 5 mg/$g_{catalyst}$. Apparently, at 250 °C the oxidation activity of the noble metals and the SSA seem to be the crucial factors for NO_x adsorption, while at 350 °C the stability of the adsorbed NO_x species plays an increasingly important role.

The stability of the stored NO_x was investigated by applying TPD to the samples saturated with NO_x at 250 °C. An example of such a TPD experiment is shown in Fig. 8, where both DTG and the MS traces of NO ($m/z = 30$) are presented. The observed mass loss (DTG) originated primarily from the evolution of NO_x from the material, although at lower temperatures (250–400 °C) desorption of water might also have contributed. Taking the evolution of NO as measure of the thermal stability of the stored NO_x, Fig. 8 shows some surprising differences. Evolution of NO increased smoothly until a maximal rate of desorption was reached at ca. 390, 410 and 450 °C for $Rh/MgAl_2O_4$, $Pt/MgAl_2O_4$ and $Pd/MgAl_2O_4$, respectively. The rather broad NO signals point to the presence of several different NO_x species and the significant differences in maximal rate of desorption indicates different strengths of adsorption. Note that the

Table 2
NO_x uptake of $M/MgAl_2O_4$ catalysts in mg NO_x/g catalyst at different temperatures.

Catalyst	Uptake	
	At 250 °C	At 350 °C
$Pt/MgAl_2O_4$	25	9
$Pd/MgAl_2O_4$	20	10
$Rh/MgAl_2O_4$	20	5

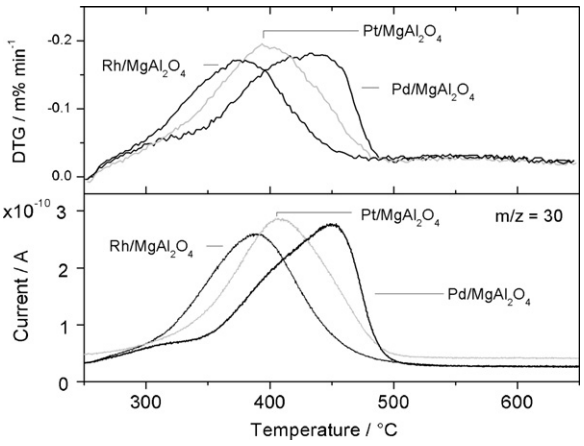

Fig. 8. Gravimetric (DTG) and mass spectrometric investigation of NO ($m/z = 30$) desorption from $M/MgAl_2O_4$ catalysts previously saturated with NO_x at 250 °C.

presence of several adsorbed NO_x species has also been evidenced by the DRIFT spectra in Fig. 5 (*vide supra*).

If we assume the maximal rate of NO_x desorption (peak temperature) to be a measure of the stability of the adsorbed NO_x-species, then we can conclude from Fig. 8 that firstly the stabilities are not equal, and that the order in stability seems to be $Pd/MgAl_2O_4 > Pt/MgAl_2O_4 > Rh/MgAl_2O_4$. This is the same order as found for the maximal NO_x storage at 350 °C (Table 2).

The difference in thermal stabilities could originate either from the different intrinsic decomposition activity of the noble metals and/or from the different relative abundance of adsorbed NO_x species (see Fig. 5).

Since Mg at the surface is a prime requirement for efficient NO_x storage of the $MgAl_2O_4$ supported catalysts, partial incorporation of the noble metal constituent [26], which depending on the synthesis protocol used cannot be ruled out completely, could alter the NO_x storage capabilities.

3.5. NO_x reduction

Next, we investigated the reduction behavior of the three NO_x saturated catalysts. The reduction of stored NO_x was examined with three different reductants: H_2, CO and C_3H_6. Prior to reduction, NO_x was stored on the catalysts by exposure to a flow of NO/O_2 in He balance at 350 °C for 15 min, after which the catalyst was exposed to a reductant flow for 45 min. Fig. 9 shows DRIFT spectra taken during the reduction of stored NO_x on $M/MgAl_2O_4$ (M = Pt, Rh or Pd) by H_2. As seen in Fig. 9 (top), $Pt/MgAl_2O_4$ showed incomplete reduction even after 45 min; the band intensity at 1290 cm^{-1} (chelating bidentate nitrate) decreased by only 45%. Besides, a new band emerged gradually at 2050 cm^{-1}, which is assigned to on-top CO adsorbed on Pt. In the gas mixture ($NO + O_2$, H_2), there was no carbon source. Therefore, the CO formation is considered to originate from the residual carbonaceous species after the FSP synthesis as described in Section 3.1. During the reduction, H_2O is produced together with N_2, N_2O and NH_3 [33]. The produced H_2O may react with the residual carbon in a steam reforming reaction to form H_2 and CO, which adsorbs strongly on the Pt surface. For $Rh/MgAl_2O_4$ complete reduction of the stored NO_x was confirmed, suggesting that the reduction efficiency of $Rh/MgAl_2O_4$ is higher than that of $Pt/MgAl_2O_4$. It should be noted that absorption bands of on-top and bridged CO on Rh emerged at 1990 and 1818 cm^{-1}, whose band positions were much lower than those of a conventional Rh catalyst, e.g., 2020–2090 cm^{-1} for on-top CO and 1830–1900 cm^{-1} for bridged CO [34]. In addition, no blue shift resulting from dipole–dipole interaction between CO molecules

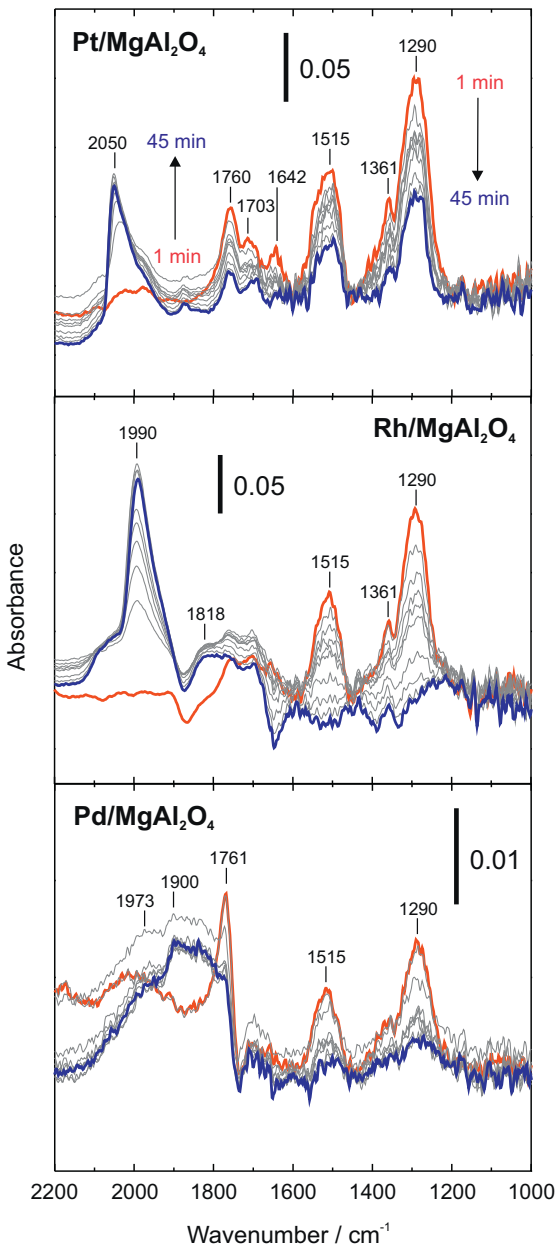

Fig. 9. Time-resolved DRIFT spectra (1–45 min) during rich period (5 vol.% H_2 in He balance) over 1 wt% $M/MgAl_2O_4$ (M = Pt, Pd or Rh) at 350 °C (Color on Web).

was observed. Taking into account these facts, the absorption bands at 1990 and 1818 cm^{-1} can be assigned to on-top and bridged $Rh_2(CO)_3$ species, indicating that some Rh atoms existed as small clusters, e.g., dimers [35,36]. This also corroborates the higher CO uptake (CO/M = 0.75) in Table 1. The reduction behavior of $Pd/MgAl_2O_4$ showed similar trend as $Pt/MgAl_2O_4$, such as incomplete reduction as seen in Fig. 9 (bottom). The formation of CO adsorbed on Pd was also observed at ca. 1973 and 1990 cm^{-1} as bridged and three-fold CO, respectively.

Fig. 10 shows the efficiency of NO_x (nitrate) reduction by H_2 over the three catalysts as a function of time calculated on the basis of the band area of chelating bidentate nitrate (1290 cm^{-1}) in Fig. 9. The intensity decrease of the other band at 1515 cm^{-1} followed a similar trend to the one at 1290 cm^{-1} for all three catalysts, whereas the band at 1760 cm^{-1} ($\nu_1 + \nu_4$) decreased with a slight time-delay (not shown). This confirms that the reduction of the bulk species occurred more slowly than the reduction of the

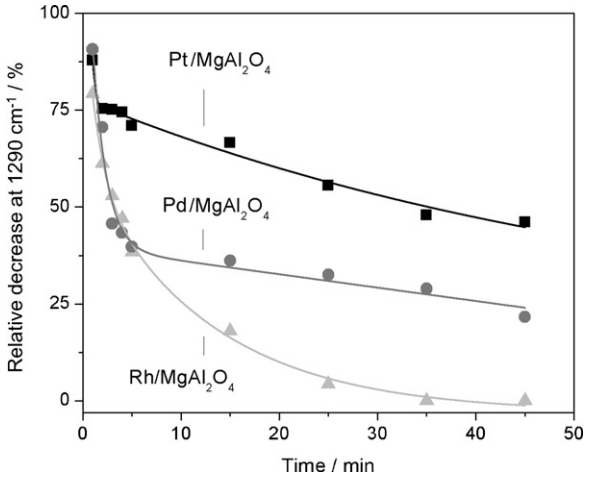

Fig. 10. Decrease of NO_x previously stored on $M/MgAl_2O_4$ measured by decrease of intensity of the band at 1290 cm^{-1} during reduction with H_2 at 350 °C.

surface species. According to Fig. 10, the reduction rate follows the order $Rh/MgAl_2O_4 > Pd/MgAl_2O_4 > Pt/MgAl_2O_4$. This order is in line with the intrinsic NO_x reduction activity of the noble metals [3,4] and their different dispersions (Table 1). However, it should be stressed that at the same metal loading (1 wt%) and similar metal dispersion the number of surface atoms is almost double for Rh and Pd than for Pt due to their much lower relative atomic mass (Rh: 102.91, Pd: 106.42, Pt: 195.08 g/mol). In this light the given orders of oxidation and reduction efficiencies of the catalysts are not rigorously reflecting intrinsic activities of the metal constituents, but the performances of catalysts with 1 wt% metal loadings.

3.6. Reduction with CO or C_3H_6

Next, we investigated the reduction of stored NO_x species by CO or C_3H_6 using in situ DRIFTS. Prior to flowing 5 vol.% CO/He or C_3H_6/He, the catalysts were saturated with NO_x in a flow of 1000 ppm NO and 6.6 vol.% O_2 in He balance at 350 °C for 15 min. Compared to reduction with H_2 (Fig. 9), the spectra obtained during reduction by C_3H_6 and CO were more complicated. Fig. 11 presents DRIFT spectra measured during the reduction over $Rh/MgAl_2O_4$. The DRIFT spectra for $Pt/MgAl_2O_4$ and $Pd/MgAl_2O_4$ were rather complicated and less conclusive and are therefore not shown here. The bands assignable to chelating bidentate nitrate at 1290 and 1515 cm^{-1} decreased less slowly for both C_3H_6 and CO than for the H_2 reduction (Fig. 9). New bands at 2069, 2214 cm^{-1}, due to Rh–CO and isocyanate (–NCO), respectively, emerged during reduction with C_3H_6. During reduction with H_2 (Fig. 9), small clusters such as $Rh_2(CO)_3$ dimer species dominated, whereas during reduction with C_3H_6 the Rh clusters appeared to agglomerate into larger particles, e.g. Rh_x–CO as evidenced by the band at 2069 cm^{-1} [34].

The spectral feature completely differed for the reduction with CO (Fig. 11, bottom). Major bands for adsorbed CO appeared as a twin peak at 2008 and 2080 cm^{-1} together with a shoulder at around 2060 cm^{-1}, which is assigned to CO adsorbed on metallic Rh. The twin peak can be assigned to asymmetric and symmetric stretching vibrations of $Rh^+(CO)_2$ [34]. Therefore, cationic Rh atoms are considered to be well-dispersed on the surface under the CO atmosphere. Interestingly, the bands assigned to isocyanate species (–NCO) at 2214 and 2250 cm^{-1} [37,38] behaved as intermediate species; in the first 3 min, the band intensity increased rapidly and then decreased gradually until 45 min of reduction. The involvement of isocyanate species as a key intermediate in the NO reduction by CO was thoroughly studied by other group [39,40]. Therefore, it is reasonable to consider that the reduction of the

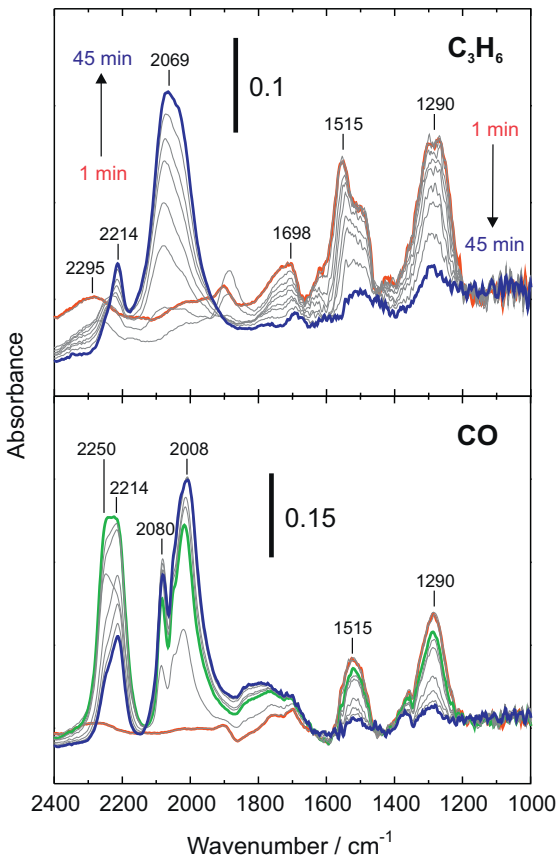

Fig. 11. Time-resolved DRIFT spectra (1–45 min) during different rich periods over 1 wt% $M/MgAl_2O_4$ (M = Pt, Rh and Pd) using 5 vol.% C_3H_6/He (top) or CO/He (bottom) at 350 °C (Color on Web).

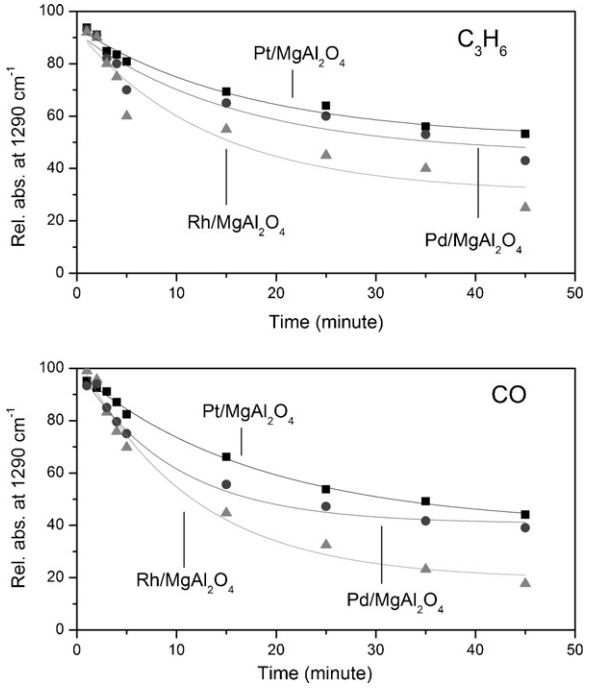

Fig. 12. Decrease of NO_x previously stored on $M/MgAl_2O_4$ measured by decrease of intensity of the band at 1290 cm^{-1} during reduction with 5 vol.% C_3H_6/He (top) and CO/He (bottom) at 350 °C.

stored NO_x on $Rh/MgAl_2O_4$ with CO as a reductant also proceeds through the isocyanate route, at least under conditions of low water content in the feed.

Fig. 12 shows a comparison of the reduction efficiency of CO and C_3H_6 over the three catalysts. Again, these plots were made by monitoring the change in the area under the major band at 1290 cm^{-1} with time. When CO or C_3H_6 were used as reductant, the order in reduction efficiency was: $Rh/MgAl_2O_4 > Pd/MgAl_2O_4 > Pt/MgAl_2O_4$. Note that, during the first phase of reduction, the reduction efficiency of all three catalysts seemed to be similar. However, the difference of reduction efficiency becomes prominent when the reductants are passed over the catalysts for longer time which might indicate that the catalysts are differently affected by adsorbed carbonaceous surface species evolving during the reduction process.

From the above results it emerges that $Pt/MgAl_2O_4$ is the most efficient catalyst for NO_x oxidation and storage, but it has the poorest reduction ability, independent whether H_2 or any of the carbonaceous reductants (CO, propene) were used. On the other hand, $Rh/MgAl_2O_4$ was most efficient for reduction of stored NO_x irrespective of the reductant used. Future work will focus on the long term behavior of these catalysts during cycling operation and on the effect of sulfur, CO_2 and water.

4. Conclusions

$MgAl_2O_4$ spinel-based catalysts with 1 wt% noble metal (Pt, Pd, Rh) were prepared by single step flame spray pyrolysis under identical conditions. The $MgAl_2O_4$ constituent of the catalysts showed similar structural characteristics, while the noble metal dispersion varied depending on the noble metal. The performances of the catalysts in NO oxidation, storage and subsequent reduction with either H_2, CO or C_3H_6 was investigated by time-resolved IR spectroscopy and gravimetric techniques. At 250 °C, the total amount of stored NO_x correlated with the specific surface areas of the catalysts. At 350 °C this behavior changed, and the stability of NO_x seemed to determine the maximal storage of NO_x. TPD analysis of the stored NO_x species revealed significant differences of their thermal stability, being highest on $Pd/MgAl_2O_4$ and lowest on $Rh/MgAl_2O_4$.

The reduction behavior of the NO_x saturated catalysts depended strongly on the reductant employed: in case of H_2, $Pt/MgAl_2O_4$ proved superior, especially at short reduction (regeneration) times (<50 s). This behavior changed when CO or C_3H_6 were used as reductants, in these cases $Rh/MgAl_2O_4$ was superior, especially at longer regeneration times.

Acknowledgments

We kindly acknowledge financial support by ETH Zurich (TH-09 06-2). We thank Dr. Frank Krumeich for the electron microscopy study, which was performed at EMEZ (Electron Microscopy ETH Zurich).

References

[1] S. Matsumoto, Catal. Today 29 (1996) 43–45.
[2] N. Takahashi, H. Shinjoh, T. Iijima, T. Suzuki, K. Yamazaki, K. Yokota, H. Suzuki, N. Miyoshi, S. Matsumoto, T. Tanizawa, T. Tanaka, S. Tateishi, K. Kasahara, Catal. Today 27 (1996) 63–69.
[3] W.S. Epling, L.E. Campbell, A. Yezerets, N.W. Currier, J.E. Parks, Catal. Rev. Sci. Eng. 46 (2004) 163–245.
[4] S. Roy, A. Baiker, Chem. Rev. 109 (2009) 4054–4091.
[5] R. Burch, Catal. Rev. Sci. Eng. 46 (2004) 271–333.
[6] Y.J. Li, S. Roth, J. Dettling, T. Beutel, Top. Catal. 16 (2001) 139–144.
[7] W.S. Epling, A. Yezerets, N.W. Currier, Catal. Lett. 110 (2006) 143–148.
[8] J.S. Choi, W.P. Partridge, C.S. Daw, Appl. Catal. A 293 (2005) 24–40.
[9] J.S. Choi, W.P. Partridge, C.S. Daw, Appl. Catal. B 77 (2007) 145–156.
[10] N. Takahashi, K. Yamazaki, H. Sobukawa, H. Shinjoh, Appl. Catal. B 70 (2007) 198–204.
[11] J.P. Breen, C. Rioche, R. Burch, C. Hardacre, F.C. Meunier, Appl. Catal. B 72 (2007) 178–186.
[12] T. Szailer, J.H. Kwak, D.H. Kim, J. Szanyi, C.M. Wang, C.H.F. Peden, Catal. Today 114 (2006) 86–93.
[13] D.H. Kim, Y.H. Chin, J.H. Kwak, C.H.F. Peden, Catal. Lett. 124 (2008) 39–45.
[14] H. Abdulhamid, E. Fridell, J. Dawody, M. Skoglundh, J. Catal. 241 (2006) 200–210.
[15] A. Amberntsson, M. Skoglundh, S. Ljungstrom, E. Fridell, J. Catal. 217 (2003) 253–263.
[16] W.S. Epling, G.C. Campbell, J.E. Parks, Catal. Lett. 90 (2003) 45–56.
[17] W.S. Epling, J.E. Parks, G.C. Campbell, A. Yezerets, N.W. Currier, L.E. Campbell, Catal. Today 96 (2004) 21–30.
[18] C.M.L. Scholz, V.R. Gangwal, M.H.J.M. de Croon, J.C. Schouten, Appl. Catal. B 71 (2007) 143–150.
[19] L. Lietti, P. Forzatti, I. Nova, E. Tronconi, J. Catal. 204 (2001) 175–191.
[20] S. Roy, N. van Vegten, A. Baiker, J. Catal. 271 (2010) 125–131.
[21] H. Abdulhamid, E. Fridell, M. Skoglundh, Appl. Catal. B: Environ. 62 (2006) 319–328.
[22] R. Strobel, L. Madler, M. Piacentini, M. Maciejewski, A. Baiker, S.E. Pratsinis, Chem. Mater. 18 (2006) 2532–2537.
[23] B. Schimmoeller, S.E. Pratsinis, A. Baiker, ChemCatChem 3 (2011) 1234–1256.
[24] A. Urakawa, N. Maeda, A. Baiker, Angew. Chem. Int. Ed. 47 (2008) 9256–9259.
[25] M.O. Symalla, A. Drochner, H. Vogel, R. Büchel, S.E. Pratsinis, A. Baiker, Appl. Catal. B 89 (2009) 41–48.
[26] N. van Vegten, M. Maciejewski, F. Krumeich, A. Baiker, Appl. Catal. B 93 (2009) 38–49.
[27] J.J.F. Scholten, A.P. Pijpers, A.M.L. Hustings, Catal. Rev. Sci. Eng. 27 (1985) 151–206.
[28] H. Hesske, A. Urakawa, A. Baiker, J. Phys. Chem. C 114 (2010) 15042–15048.
[29] C. Sedlmair, K. Seshan, A. Jentys, J.A. Lercher, J. Catal. 214 (2003) 308–316.
[30] J.B. Yu, Z. Jiang, L. Zhu, Z.P. Hao, Z.P. Xu, J. Phys. Chem. B 110 (2006) 4291–4300.
[31] S. Morandi, F. Prinetto, G. Ghiotti, M. Livi, A. Vaccari, Micropor. Mesopor. 107 (2008) 31–38.
[32] F. Prinetto, G. Ghiotti, I. Nova, L. Lietti, E. Tronconi, P. Forzatti, J. Phys. Chem. B 105 (2001) 12732–12745.
[33] L. Lietti, I. Nova, P. Forzatti, J. Catal. 257 (2008) 270–282.
[34] B.E. Hayden, A. King, M.A. Newton, N. Yoshikawa, J. Mol. Catal. A: Chem. 167 (2001) 33–46.
[35] J.C.S. Wong, J.T. Yates, J. Am. Chem. Soc. 116 (1994) 1610–1615.
[36] J.C.S. Wong, J.T. Yates, J. Phys. Chem. 99 (1995) 12640–12646.
[37] T. Szailer, J.H. Kwak, D.H. Kim, J.C. Hanson, C.H.F. Peden, J. Szanyi, J. Catal. 239 (2006) 51–64.
[38] H. Abdulhamid, J. Dawody, E. Fridell, M. Skoglundh, J. Catal. 244 (2006) 169–182.
[39] T. Hirano, Y. Ozawa, T. Sekido, T. Ogino, T. Miyao, S. Naito, Catal. Commun. 8 (2007) 1249–1254.
[40] T. Hirano, Y. Ozawa, T. Sekido, T. Ogino, T. Miyao, S. Naito, Appl. Catal. A: Gen. 320 (2007) 91–97.